Article ID: 1000-324X(2023)03-0357-06 **DOI:** 10.15541/jim20220504

Luminescence Property and Judd-Ofelt Analysis of 0.6%Pr, *x*%La:CaF_2 Crystals

QIAN Xinyu[1,2], WANG Wudi[2], SONG Qingsong[2], DONG Yongjun[4], XUE Yanyan[2], ZHANG Chenbo[2], WANG Qingguo[2], XU Xiaodong[3], TANG Huili[2], CAO Guixin[1], XU Jun[2]

(1. Materials Genome Institute, Shanghai University, Shanghai 200444, China; 2. Key Laboratory of Advanced Micro-Structured Materials of Ministry of Education, School of Physics Science and Engineering, Institute for Advanced Study, Tongji University, Shanghai 200092, China; 3. Jiangsu Key Laboratory of Advanced Laser Materials and Devices, School of Physics and Electronic Engineering, Jiangsu Normal University, Xuzhou 221116, China; 4. Nanjing Metalaser Photonics Company Ltd., Nanjing 210038, China)

Abstract: Calcium fluoride (CaF_2) is an attractive laser material due to its broad transmission range (0.125–10 μm), good thermal conductivity (9.71 W/(m·K)) and low coefficient of nonlinear effect. In Pr:CaF_2 crystal, the [Pr^{3+}-Pr^{3+}] cluster lead to fluorescence quenching at lower concentrations of Pr^{3+} ions. Therefore, co-doping of La ions in CaF_2 to break the [Pr^{3+}-Pr^{3+}] cluster deserves further exploration. In this work, a series of Pr:CaF_2 single crystals co-doped with different concertation of La^{3+} ions were successfully grown by temperature gradient technique (TGT). The X-ray powder diffraction, absorption spectra, fluorescence spectra and fluorescence decay lifetime of Pr,La:CaF_2 crystals were measured. Obtained data demonstrated that the Pr:CaF_2 crystals still had the cubic crystal structure after co-doped with La^{3+} ions. The largest stimulated emission cross-sections of $^3P_0\rightarrow{}^3H_6$ (604 nm) and $^3P_0\rightarrow{}^3F_2$ (640 nm) transitions were calculated to be 1.36×10^{-20} cm^2 and 3.18×10^{-20} cm^2 with FWHM of 17.0 nm and 3.8 nm, respectively. With the increase of La^{3+} ion concentration, the value of FWHM increased from 15.84 nm to 18.53 nm of $^3P_0\rightarrow{}^3H_6$. The largest fluorescent lifetime and spectral quality factor of 0.6%Pr, 10%La:CaF_2 (atom fraction) is 45.82 μs and 1.458×10^{-18} $cm^2\cdot$μs, respectively. All above results show that the [Pr^{3+}-Pr^{3+}] ions quench clusters are broken by La^{3+} ions. The Pr, La:CaF_2 crystal is a potential laser gain material for orange-red laser operation.

Key words: Pr, La:CaF_2; spectra property; Judd-Ofelt theory; fluorescence lifetime

Since the first solid-state ruby laser (Cr:Al_2O_3) was manufactured, the laser has played an important role in our life[1]. In the past few decades, with the development of GaN/InGaN laser diode (LD), the solid-state laser source at visible light range has very important prospects in various applications, such as biomedical, data storage, remote sensing and quantum optics[2-6]. Trivalent praseodymium ions (Pr^{3+}) can achieve transition emission from deep red ($^3P_0\rightarrow{}^3F_4$), red ($^3P_0\rightarrow{}^3F_2$), orange ($^3P_0\rightarrow{}^3H_6$), green ($^3P_{0,1}\rightarrow{}^3H_5$) to blue ($^3P_0\rightarrow{}^3H_4$) region due to its plentiful energy level structures[7-10]. Therefore, Pr^{3+}-doped laser materials have attracted much attention in the development process of all visible solid-state lasers[11-12].

Compared with oxide crystals, fluoride crystals have lower phonon energy and excellent mechanical properties. Among them, calcium fluoride (CaF_2) crystals have been widely concerned and studied due to their excellent thermal conductivity (9.8 W/(m·K)), wide transmission range (0.157–10 μm), low refractive index and small non-linear effects, which is the excellent laser gain medium and high transmittance window materials. In addition, calcium fluoride belongs to the cubic crystal system which is easy to obtain large-sized and high-quality single crystals. In the 1960s and 1970s, Sorokin and Stevenson, *et al* reported that the first laser output was obtained by U^{3+}[13] and Sm^{2+}[14] ion-doped calcium fluoride (CaF_2) crystals.

In trivalent praseodymium ions (Pr^{3+}) doped CaF_2 crystals, Pr^{3+} ions replace the site of divalent Ca^{2+} ions, and interstitial F^- ions are introduced into the lattice vacancies to maintain the charge balance of the lattice. Meanwhile, [Pr^{3+}-Pr^{3+}] clusters can form even at lower

Received date: 2022-08-26; **Revised date:** 2022-10-22; **Published online:** 2022-12-30
Foundation item: National Natural Science Foundation of China (61621001, 62075166, 61805177); Fundamental Research Funds for the Central Universities (22120210432)
Biography: QIAN Xinyu (1998–), male, Master candidate. E-mail: 894742295@qq.com
钱新宇(1998–), 男, 硕士研究生. E-mail: 894742295@qq.com
Corresponding author: XU Jun, professor. E-mail: xujun@mail.shcnc.ac.cn
徐 军, 教授. E-mail: xujun@mail.shcnc.ac.cn

Pr^{3+} ions doping concentration due to the dipole interaction between Pr^{3+} and F^- ions, which leads to the fluorescence quench. Therefore, a new mixed fluoride crystals system by co-doping R^{3+} (R= La^{3+}, Y^{3+}, Lu^{3+} and Gd^{3+}) is designed to break clusters and release more luminescent centers. Compared with Pr^{3+} ions single doped, Pr^{3+}:RF_3-CaF_2 (R= La^{3+}, Y^{3+}, Lu^{3+} and Gd^{3+}) crystals have better spectral property. As for Pr:YF_3-CaF_2 crystals, Beck, *et al*[15] reported that the emission intensity has been greatly increased and crystals show inhomogeneous and broad emission spectrum characteristics of glasses. The incorporation of La^{3+} ions could reduce fluorescence quenching in fluorites[16]. In CaF_2 crystals, the luminescence intensity of Pr^{3+} ions is also enhanced by co-doping Lu^{3+} ions[17]. The red laser output power at 642 nm reaches 22.2 mW, and the slope efficiency is 7.5% in CaF_2 crystal by co-doping Gd^{3+} ions[4].

In present work, a series of Pr:CaF_2 crystals co-doping different concertation of La^{3+} ions were successfully grown by the temperature gradient technique (TGT). The modulation effects of different concentrations of La^{3+} ions on the spectral property and Judd-Ofelt (J-O) theory analysis crystals were studied and analyzed.

1 Experimental

A series of Pr:CaF_2 crystals by co-doping different concertation La^{3+} ions were successfully grown by TGT, as shown in Fig. 1. In previous experiments, we found that concentration quenching effect of Pr^{3+} ions occurred at concentrations above 0.6% in CaF_2 crystal. Therefore, high purity of PrF_3 (99.99%), LaF_3 (99.99%) and CaF_2 (99.99%) were used as raw materials and weighted according to the formula: 0.6%Pr, x%La:CaF_2 (x=3, 10, 18). These raw powders were grounded about 30 min in an agate mortar. Then the raw materials were put into a porous graphite crucible in the cylindrical part. After the chamber was vacuumed to 15 Pa, the entire chamber was filled with high-argon gas to 110 kPa. The temperature was raised to 1430 ℃ for 6 h until the raw powders melted completely. The crystal grown procedure was controlled at the rate of 1 ℃/h. After crystals grown, slices were cut from the middle part of crystal and double-side polished to 1 mm thickness

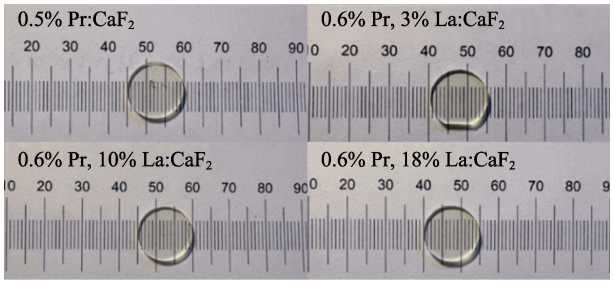

Fig. 1 As-grown 0.6%Pr, x%La:CaF_2 (x=3, 10, 18) single crystals

The structure of Pr,La:CaF_2 crystals were studied and analyzed by X-ray powder diffraction (XRD) using Ultima IV diffractometer with a step size of 0.02°. The concentrations of Pr^{3+} and La^{3+} ions were analyzed by inductively coupled plasma atomic emission spectrometry (ICP-AES). At room temperature, the absorption spectra of 400–2500 nm were tested by using a UV-VIS-NIR spectrophotometer (Lambda 900, Perkin-Elmer). The room temperature fluorescence spectra of 450–800 nm and fluorescence lifetime at 483 nm were measured by a FLS-1000 fluorescence spectrometer (Edinburgh Company, English).

2 Results and discussion

2.1 XRD and ICP-AES analysis

The samples of XRD were cut from as-grown crystals and grounded into powder. Fig. 2 shows XRD patterns of Pr,La:CaF_2 crystals. The diffraction peak position and intensity of 0.6%Pr, x%La:CaF_2 (x=0, 3, 10, 18) were consistent with that of pure CaF_2 crystal. This means that no other impurity phase is generated. From XRD pattern, the lattice parameter a of 0.6%Pr, x%La:CaF_2 (x=0, 3, 10, 18) were calculated to be 0.54727, 0.54851, 0.55192, 0.55606 nm. The result show that the lattice parameters of Pr, La:CaF_2 increased with increasing of doping concentration of La^{3+} ions, The lattice parameters are increased when Pr^{3+} and La^{3+} ions entry into lattice replace Ca^{2+} (0.100 nm) sites. The interstitial F^- ions (0.133 nm) are introduced to keep the balance of the system[17].

As shown in Table S1, the concentration of Pr^{3+} and La^{3+} ions were tested by ICP-AES. The result shows that actual concentration of Pr^{3+} and La^{3+} are closed to initial concentration. The segregation coefficient of Pr,La:CaF_2 are closed to 1, which shows that the dopant ions are

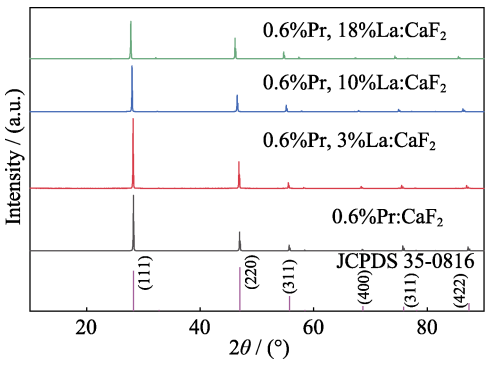

Fig. 2 XRD patterns of Pr,La:CaF_2 crystals and standard pattern of CaF_2 crystal

uniformly distributed in the host material and Pr,La:CaF_2 crystal have good quality.

2.2 Absorption spectra

The room temperature absorption spectra of Pr,La:CaF_2 crystals from 400 to 2500 nm show in Fig. 3. There are eight absorption bands of Pr^{3+} ions, corresponding to transitions from ground state of $^3H_4$ to excited states of $^3P_2$, $^3P_1$, $^3P_0$, $^1D_2$, $^3F_4$, $^3F_3$, $^3F_2$ and $^3H_6$, respectively. In the blue visible region of 440–480 nm, absorption peak positions are 442 or 443 nm, corresponding to absorption transition of $^3H_4 \rightarrow {}^3P_2$. The absorption peak matches the emission wavelength of the high-efficiency blue laser diode. The absorption cross-section $\sigma_{abs}(\lambda)$ can be calculated by the following formula:

$$\sigma_{abs}(\lambda) = \frac{2.303}{N_0 \times L} \mathrm{OD}(\lambda) \quad (1)$$

Where $\mathrm{OD}(\lambda)$ is the optical density, N_0 is actual concentration of Pr^{3+} ion, λ is wavelength and L is the thickness of these samples. Among all samples, 0.6%Pr,10% La:CaF_2 has the largest absorption cross-section reaching 1.743×10^{-20} cm^2. The large absorption cross-section is very favorable for the absorption of pump wavelength.

2.3 Judd-Ofelt theory analysis

In 1962, in order to explain the energy level transition of rare earth ions, the Judd-Ofelt (J-O) theory was proposed[18-19], which is now widely used to analyze the spectral properties of rare earth ions in host materials.

For Pr^{3+} ions, magnetic-dipole (MD) transitions is forbidden because transition rule is not complied, therefore electric-dipole (ED) transitions is only considered[20-21]. The selection rules of MD transition in the lanthanides are: $\Delta S=\Delta L=0$, $\Delta J=0, \pm1$. According to these rules, Pr^{3+} ions does not satisfy the selection rule of MD transition. So the magnetic-dipole transitions would not be taken into account in the calculations of spectroscopic parameters of the Pr,La:CaF_2 crystal. According to J-O theory, the calculated line strength $S_{cal}(J\rightarrow J')$ can be expressed as following formula:

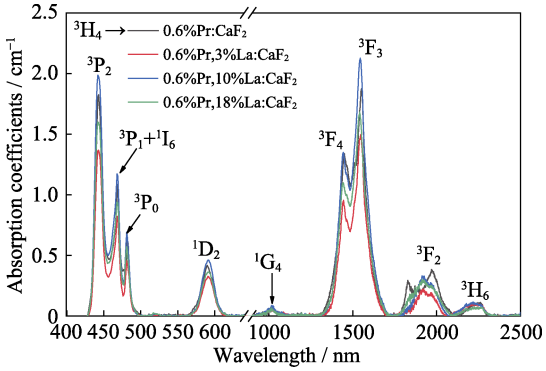

Fig. 3　Absorption spectra of Pr,La:CaF_2 crystals at room temperature

Colorful figure is available on website

$$S_{cal}(J\rightarrow J') = \sum_{t=2,4,6} \Omega_t \left| \left\langle S,L,J \| U^{(t)} \| S',L',J' \right\rangle \right|^2 \quad (2)$$

Where J and J' are the angular momentum quantum numbers of the initial and final levels, $\|U^{(t)}\|$ is the squared reduced matrix elements of the tensorial operator, $\Omega_t (t = 2, 4, 6)$ are the J-O intensity parameters.

The experiments line strength $S_{exp}(J\rightarrow J')$ of ED transitions can also be expressed as following formula:

$$S_{exp}(J\rightarrow J') = \frac{3hc(2J+1)}{8\pi^3 e^3 N} \frac{9n}{(n^2+2)^2} \frac{1}{L\bar{\lambda}} \times \int \mathrm{OD}(\lambda)\mathrm{d}\lambda \quad (3)$$

Where h is the Planck constant, c is the speed of light in vacuum, e is the electron charge, N is the concentration of Pr^{3+} ion doping, n represents the refractive index of the Pr,La:CaF_2 crystal, λ is the average wavelength of the absorption band, L is the thickness of the samples, and $\mathrm{OD}(\lambda)$ represents optical density.

The root-mean-square (RMS) deviation between the experiment line strengths $S_{exp}(J\rightarrow J')$ and calculation line strengths $S_{cal}(J\rightarrow J')$ can be defined as the following formula:

$$\mathrm{RMS}\Delta S = \sqrt{\sum_{J'} (S_{exp} - S_{cal})^2 / (P-3)} \quad (4)$$

Where P is the number of absorption bands in the process of calculation. For 0.6% Pr, x% La:CaF_2 (x=3, 10, 18) crystals, the average wavelength λ, absorption line strength $S_{exp}(J, J')$, calculated line strength $S_{cal}(J, J')$ and RMSΔS are calculated by the formula (2–4), as shown in Table S2. The value of RMSΔS is 0.744×10^{-20}, 0.290×10^{-20}, and 0.793×10^{-20} cm^2, respectively.

The J-O intensity parameters Ω_t (t=2, 4, 6) of Pr,La:CaF_2 crystals and other host crystals are compared and shown in Table S3. For J-O intensity parameters Ω_t (t=2, 4, 6), Ω_2 is represents the symmetry and covalent bond strength of the Pr^{3+} ions coordination structure. The value of $\Omega_2(1.68\times10^{-20}$ $cm^2)$ of Pr,La:CaF_2 crystals is higher than those of LaF_3[22], BaY_2F_8[23], $Y_3Al_5O_{12}$[24] and $SrAl_{11}O_{19}$[25], but smaller than those of LYF_4[22], KYF_4[23], and $CaYAlO_4$[26]. Ω_4 and Ω_6 represent the whole performance of crystals such as rigidity and viscosity of matrix. Ω_4/Ω_6 is spectroscopic quality factor that can indicate the stimulated emission efficiency in the laser gain medium[27]. It can be found that the value of $\Omega_4/\Omega_6(0.61)$ of CaF_2 crystal is higher than those of LYF_4[22], KYF_4[23] and $SrAl_{11}O_{19}$[25] crystal from Table S3.

The radiative transition rates $A(J\rightarrow J')$ from the excited state $^3P_0$ to other lower state is defined by following formula:

$$A(J\rightarrow J') = A^{ed} + A^{em}$$

$$A^{ed} = \frac{64\pi^4 e^2 n(n^2+2)^2}{27h(2J+1)\bar{\lambda}^3} \sum_{t=2,4,6} \Omega_t \left| \left\langle S,L,J \| U^{(t)} \| S',L',J' \right\rangle \right|^2 \quad (5)$$

$$A^{md} = \frac{64\pi^4 e^2}{3h(2J+1)\bar{\lambda}^3} S^{md} \quad (6)$$

$$A(J\to J')=\frac{64\pi^4e^2}{3h(2J+1)\bar{\lambda}^3}\left(\frac{n(n^2+2)^2}{9}S^{\mathrm{ed}}+S^{\mathrm{md}}\right) \quad (7)$$

Where $\|U^{(t)}\|=2,4,6$ (t=2,4,6) is the emission squared reduced matrix elements of the tensorial operator, which is shown in Ref. [21]. A^{ed} is the probability of electric-dipole transitions. A^{md} is the probability of magnetic-dipole transitions. S^{md} is the magnetic dipole radiation intensity, which is an independent constant. S^{md} is ignored due to the forbidden of magnetic-dipole transitions for Pr^{3+} ions. S^{ed} is the electric dipole radiation intensity which could be defined by following formula:

$$S^{\mathrm{ed}}=\sum_{t=2,4,6}\Omega_t\cdot U_t \quad (8)$$

The fluorescence branching ratio ($\beta_{JJ'}$) and radiation lifetime (τ_{rad}) can be calculated by the following formula:

$$\beta_{JJ'}=\frac{A(J\to J')}{\sum_{J'}A(J\to J')} \quad (9)$$

$$\tau_{\mathrm{rad}}=\frac{1}{\sum_{J'}A(J\to J')} \quad (10)$$

The spontaneous transition rate, branch ratio and radiation lifetime of the $^3P_0$ energy level in Pr,La:CaF_2 crystals are shown in Table S4. For $^3P_0$ energy level, the radiation lifetime of 0.6% Pr, x% La:CaF_2 (x=0, 3, 10 and 18) crystals are 137.3, 201.1, 136.3, and 168.9 μs, respectively. The radiation lifetime is longer than those of Pr^{3+}:$SrWO_4$ (9.5 μs)[28], Pr:$KLu(WO_4)_2$ (10.18 μs)[29], Pr:$YAlO_3$ (19.99 μs)[30], Pr^{3+}:$CaYAlO_4$ (10.19 μs)[26], Pr^{3+}:$LiYF_4$ (37 μs), Pr^{3+}:KYF_4 (54 μs) and Pr^{3+}:BaY_2F_8 (54 μs)[23]. The results represent that Pr,La:CaF_2 has high energy storage capacity, which is relatively easy to realize laser operation of $^3P_0$ energy level.

2.4 Fluorescent spectra

The visible fluorescent spectra of 0.6%Pr, x% La:CaF_2 (x=0, 3, 10, 18) crystals under excitation of 443 nm is shown in Fig. 4. It can be seen that there are six emission spectra bands, which correspond to transition of $^3P_0\to{}^3H_4$(484 nm), $^3P_0\to{}^3H_5$ (537 nm), $^3P_0\to{}^3H_6$ (599 nm), $^3P_0\to{}^3F_2$ (640 nm), $^3P_0\to{}^3F_3$ (700 nm), and $^3P_0\to{}^3F_4$ (723 nm).

Stimulated emission cross section is one of the important parameters, which is usually used to evaluate laser performance of crystal. The stimulated emission cross section can be calculated by the Füchtbauere Ladenburg (F-L) formula combining the emission spectrum[31]:

$$\sigma_{\mathrm{em}}(\lambda)_{JJ'}=\frac{A(J\to J')\lambda^5}{8\pi n^2c}\frac{I(\lambda)}{\int_{\mathrm{band}}\lambda I(\lambda)\mathrm{d}\lambda} \quad (11)$$

Where $A(J\to J')$ is the radiative transition rates, $I(\lambda)$ is the experimental fluorescent intensity at the wavelength λ, c presents the light velocity, n stands for the refractive index. The peak wavelength λ, FWHM and stimulated emission cross section σ_{em} are shown in Table S5. For 0.6%Pr,10%La:CaF_2 crystal, the largest stimulated emission cross section at 640 nm reaches 3.18×10^{-20} cm^2 with FWHM of 6.8 nm, corresponding to the $^3P_0\to{}^3F_2$ transition. Furthermore, the stimulated emission cross section and FWHM of $^3P_0\to{}^3H_6$ transition are 1.36×10^{-20} cm^2 and 16.98 nm, respectively. The FWHMs of $^3P_0\to{}^3F_2$ and $^3P_0\to{}^3H_6$ transition are larger than those of Pr:$YLiF_4$, Pr:$LuLiF_4$, Pr:BaY_2F_8, Pr:$GdLiF_4$ and Pr:LaF_3[22,31-33]. With La^{3+} ions concentration increasing, FWHM increases from 15.84 to 18.53 nm for $^3P_0\to{}^3H_6$ transition. FWHM of emission band is mainly broadened by the Stark splitting of different energy level. After co-doping La^{3+}, La^{3+} ion interacts with the inherent electric dipole moment of the matrix, which enhances the electron-phonon interaction, resulting in the increasing of energy level splitting of La^{3+}, and the closed energy levels of Stark splitting overlap each other, which lead to the broadening of corresponding emission peaks. This result indicate that co-doping with La^{3+} ions facilitate the ultrafast orange laser output of Pr:CaF_2 crystals.

From Fig. 4 and Table S5, the fluorescence intensity can be greatly enhanced by co-doping with La^{3+} ions, which is due to the fact that the [Pr^{3+}-Pr^{3+}] cluster is broken, more fluorescence centers are released and thus decreasing the probability of energy transfer among luminescence center ions. It is worth noting that co-doping with La^{3+} ions can significantly improve the emission coefficients. The results indicates that the Pr,La:CaF_2 crystals display great potential to realize laser operation at orange and red light.

2.5 Fluorescent lifetime

The fluorescent lifetime decay of $^3P_0\to{}^3F_2$ transition at room temperature were measured by 443 nm Xenon lamp (Fig. 5). The fluorescence lifetime decay conforms to the characteristics of single exponential decay. The fitted

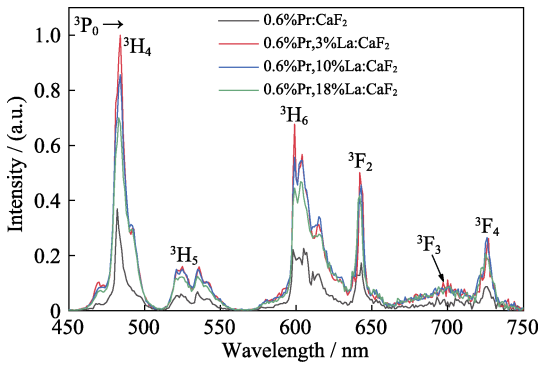

Fig. 4 Fluorescent spectra of Pr,La:CaF_2 crystals at room temperature

Colorful figure is available on website

formula is $y = y_0 + A_1 e^{-x/t_1}$. After co-doping with La^{3+} ions, the fluorescence lifetime Pr^{3+} ions are not affected only because the local coordination structure is changed. The fluorescence lifetimes of 0.6%Pr, *x*% La:CaF_2 (*x*=0, 3, 10, 18) crystals are fitted to be 43.75, 45.82, and 39.75 μs, respectively. The longest fluorescence lifetime of 0.6%Pr,10% La:CaF_2 reaches 45.82 μs, which is longer than those of Pr:$LuLiF_4$, Pr:$YLiF_4$, Pr:$GdLiF_4$ and Pr:BaY_2F_8 crystals.

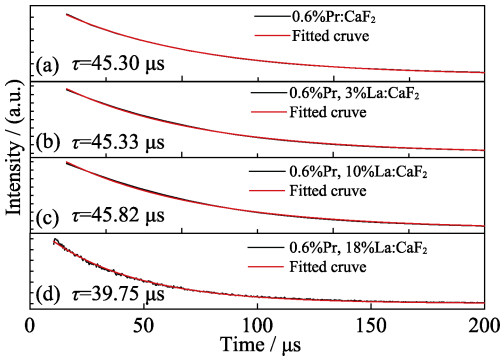

Fig. 5 Fluorescence decay lifetime of $^3P_0$ energy of 0.6%Pr, *x*%La:CaF_2 crystals at room temperature

(a) *x*=0; (b) *x*=3; (c) *x*=10; (d) *x*=18; Colorful figure is available on website

3 Conclusion

A series of Pr:CaF_2 crystals by co-doping different concertation La^{3+} ions are successfully grown by temperature gradient (TGT) method. The X-ray powder diffraction, absorption spectra, fluorescent spectra and fluorescent decay lifetime are measured and analyzed at room temperature. The largest absorption cross-sections at 442/443 nm are calculated to be 1.743×10^{-20} cm^2 of 0.6%Pr,10% La:CaF_2. The value of J-O intensity parameters Ω_2, Ω_4 and Ω_6 are fitted to 2.30×10^{-20}, 2.93×10^{-20}, and 5.84×10^{-20} cm^2, respectively. The largest stimulated emission cross-sections of $^3P_0\rightarrow{}^3H_6$ and $^3P_0\rightarrow{}^3F_2$ transitions at 604 and 640 nm are calculated to be 1.36×10^{-20} and 3.18×10^{-20} cm^2 in 0.6%Pr,10%La:CaF_2 crystal, with FWHM of 15.3 and 3.8 nm, respectively. The largest fluorescent lifetime(τ_f) and spectral quality factor ($\sigma_{em}\cdot\tau_f$) of 0.6%Pr,10%La:CaF_2 of $^3P_0\rightarrow{}^3F_2$ transition are 45.82 μs and 145.8×10^{-20} $cm^2\cdot$μs. These results show that 0.6%Pr,10%La:CaF_2 crystal is potential laser gain medium for 604 and 640 nm laser operation.

Supporting Materials

Supporting materials related to this article can be found at https://doi.org/10.15541/jim20220504.

References:

[1] MAIMAN T H. Stimulated optical radiation in ruby. *Nature*, 1960, **4736:** 493.

[2] LIU W, ZHANG Q, SUN D, *et al*. Crystal growth and spectral properties of Sm: GGG crystal. *Journal of Crystal Growth*, 2011, **331(1):** 83.

[3] REICHERT F, MARZAHL D T, HUBER G. Spectroscopic characterization and laser performance of Pr,Mg:$CaAl_{12}O_{19}$. *Journal of the Optical Society of America B*, 2014, **31(2):** 349.

[4] YU HAO, JIANG DAPENG, TANG FEI, *et al.* Enhanced photoluminescence and initial red laser operation in Pr:CaF_2 crystal *via* co-doping Gd^{3+} ions. *Materials Letters*, 2017, **206:** 140.

[5] CHEN B J, SHEN L F, PUN E Y B, *et al.* Sm^{3+}-doped germanate glass channel waveguide as light source for minimally invasive photodynamic therapy surgery. *Optics Express*, 2012, **20(2):** 879.

[6] METZ P W, MÜLLER S, REICHERT F, *et al*. Wide wavelength tunability and green laser operation of diode-pumped Pr^{3+}: KY_3F_{10}. *Optics Express*, 2013, **21(25):** 31274.

[7] WANG W, TIAN J, LI N, *et al*. Enhanced and modulated visible luminescence of Pr^{3+}:CaF_2 crystal by co-doping R^{3+} (R= Y, Gd, Lu) ions. *Journal of Alloys and Compounds*, 2021, **887:** 161327.

[8] FIBRICH M, JELÍNKOVÁ H, ŠULC J, *et al*. Diode-pumped Pr: YAP lasers. *Laser Physics Letters*, 2011, **8(8):** 559.

[9] CORNACCHIA F, RICHTER A, HEUMANN E, *et al.* Visible laser emission of solid state pumped $LiLuF_4$: Pr^{3+}. *Optics Express*, 2007, **15(3):** 992.

[10] PABŒUF D, MHIBIK O, BRETENAKER F, *et al*. Diode-pumped Pr: BaY_2F_8 continuous-wave orange laser. *Optics Letters*, 2011, **36(2):** 280.

[11] KRÄNKEL C, MARZAHL D T, MOGLIA F, *et al*. Out of the blue: semiconductor laser pumped visible rare-earth doped lasers. *Laser & Photonics Reviews*, 2016, **10(4):** 548.

[12] METZ P W, REICHERT F, MOGLIA F, *et al*. High-power red, orange, and green Pr^{3+}: $LiYF_4$ lasers. *Optics Letters*, 2014, **39(11):** 3193.

[13] SOROKIN P P, STEVENSON M J. Stimulated infrared emission from trivalent uranium. *Physical Review Letters*, 1960, **5(12):** 557.

[14] KAISER W, GARRETT C G B, WOOD D L. Fluorescence and optical maser effects in CaF_2: Sm^{2+}. *Physical Review*, 1961, **123(3):** 766.

[15] BECK W, KARASIK A, ARVANITIDIS J, *et al*. Spectral hole burning in CaF_2-YF_3:Nd^{3+} crystals. *Journal of Luminescence*, 2000, **86(3/4):** 289.

[16] KAZANSKII S A, RYSKIN A I. Clusters of group-III ions in activated fluorite-type crystals. *Physics of the Solid State*, 2002, **44(8):** 1415.

[17] SERRANO D, BRAUD A, DOUALAN J L, *et al*. Pr^{3+} cluster management in CaF_2 by codoping with Lu^{3+} or Yb^{3+} for visible lasers and quantum down-converters. *Journal of the Optical Society of America B*, 2012, **29(8):** 1854.

[18] JUDD B R. Optical absorption intensities of rare-earth ions. *Physical Review*, 1962, **127(3):** 750.

[19] OFELT G S. Intensities of crystal spectra of rare - earth ions. *The Journal of Chemical Physics*, 1962, **37(3):** 511.

[20] GUO W, LIN Y, GONG X, *et al.* Spectroscopic properties of Pr^{3+}: $KY(MoO_4)_2$ crystal as a visible laser gain medium. *Journal of Physics and Chemistry of Solids*, 2008, **69(1):** 8.

[21] BABU P, JAYASANKAR C K. Spectroscopy of Pr^{3+} ions in lithium borate and lithium fluoroborate glasses. *Physica B: Condensed Matter*, 2001, **301(3/4):** 326.

[22] LI N, XUE Y, LI D, *et al*. Crystal growth, spectral properties and Judd-Ofelt analysis of Pr: LaF_3. *Materials Research Express*, 2019, **6(11):** 116209.

[23] KHIARI S, VELAZQUEZ M, MONCORGÉ R, *et al.* Red-luminescence analysis of Pr^{3+} doped fluoride crystals. *Journal of Alloys and Compounds*, 2008, **451(1/2):** 128.
[24] MALINOWSKI M, WOLSKI R, WOLIŃSKI W. Absorption intensity analysis of Pr^{3+}: $Y_3Al_5O_{12}$. *Solid State Communications*, 1990, **74(1):** 17.
[25] OLIVEIRA A S, GOUVEIA E A, DE ARAUJO M T, *et al*. Twentyfold blue upconversion emission enhancement through thermal effects in Pr^{3+}/Yb^{3+}-codoped fluoroindate glasses excited at 1.064 μm. *Journal of Applied Physics*, 2000, **87(9):** 4274.
[26] LÜ S, WANG Y, ZHU Z, et al. Spectroscopic analysis of Pr^{3+}: $CaYAlO_4$ crystal. *Applied Physics* B, 2014, **116(1):** 83.
[27] CHEN Y, SUN D, PENG F, *et al*. Growth and spectroscopic investigations of the 1.5at% Er: GSGG laser crystal. *Materials Research Express*, 2017, **4(9):** 096202.
[28] JIA G, WANG H, LU X, *et al*. Optical properties of Pr^{3+}-doped $SrWO_4$ crystal. *Applied Physics B*, 2008, **90(3):** 497.
[29] YU Y, ZHU X, ZHANG X, *et al*. Growth and optical properties of Pr^{3+}: $KLu(WO_4)_2$ laser crystal: a candidate for red emission laser. *Optical Review*, 2016, **23(3):** 391.
[30] LIU B, SHI J, WANG Q, *et al.* Crystal growth, polarized spectroscopy and Judd-Ofelt analysis of Pr: $YAlO_3$. *Journal of Luminescence*, 2018, **196:** 76.
[31] AULL B, JENSSEN H. Vibronic interactions in Nd: YAG resulting in nonreciprocity of absorption and stimulated emission cross sections. *IEEE Journal of Quantum Electronics*, 1982, **18(5):** 925.
[32] HAKIM R, DAMAK K, TONCELLI A, *et al*. Growth, optical spectroscopy and Judd–Ofelt analysis of Pr-doped BaY_2F_8 monocrystals. *Journal of Luminescence*, 2013, **143:** 233.
[33] CORNACCHIA F, DI LIETO A, TONELLI M, *et al*. Efficient visible laser emission of GaN laser diode pumped Pr-doped fluoride scheelite crystals. *Optics Express*, 2008, **16(20):** 15932.

0.6%Pr, *x*%La:CaF_2 的发光性能研究和 Judd-Ofelt 分析

钱新宇[1,2], 王无敌[2], 宋青松[2], 董永军[4], 薛艳艳[2], 张晨波[2], 王庆国[2], 徐晓东[3], 唐慧丽[2], 曹桂新[1], 徐 军[2]

(1. 上海大学 材料基因组工程研究院, 上海 200444; 2. 同济大学 高等研究院, 物理科学与工程学院, 先进微结构材料教育部重点实验室, 上海 200092; 3. 江苏师范大学 物理与电子工程学院, 江苏省先进激光材料与器件重点实验室, 徐州 221116; 4. 南京光宝光电科技有限公司, 南京 210038)

摘 要: 氟化钙(CaF_2)是一种良好的激光材料基质, 具有较宽的透过范围(0.125~10 μm)、良好的导热性(9.71 W/(m·K))和低非线性效应系数。在 Pr:CaF_2 晶体中, [Pr^{3+}-Pr^{3+}]团簇导致 Pr^{3+}离子在较低浓度下出现荧光猝灭现象。在 CaF_2 中共掺入 La^{3+}离子有可能打破[Pr^{3+}-Pr^{3+}]团簇。本研究通过温度梯度法(Temperature Gradient Technique, TGT), 成功地生长了一系列共掺入不同浓度 La^{3+}离子的 Pr:CaF_2 晶体。在室温下采用 X 射线粉末衍射、吸收光谱、荧光光谱和荧光衰减寿命对 Pr, La:CaF_2 晶体进行表征。Pr:CaF_2 晶体共掺入 La^{3+}离子后仍具有立方晶体结构。$^3P_0\rightarrow{}^3H_6$(604 nm)和 $^3P_0\rightarrow{}^3F_2$(640 nm)处的最大受激发射截面分别为 1.36×10^{-20} 和 3.18×10^{-20} cm^2, 半峰宽分别为 17.0 和 3.8 nm。随着 La^{3+}离子掺杂含量的增加, $^3P_0\rightarrow{}^3H_6$(604 nm)处的半峰宽从 15.84 增加到 18.53 nm。0.6%Pr,10%La:CaF_2 (原子分数)的最大荧光寿命和光谱质量因子分别为 45.82 μs 和 145.8×10^{-20} $cm^2\cdot$μs。上述结果表明: [Pr^{3+}-Pr^{3+}]离子淬灭团被打破, Pr, La:CaF_2 晶体是潜在的激光增益材料, 可应用于橙红色激光领域。

关 键 词: Pr, La:CaF_2; 光谱性能; Judd–Ofelt 理论; 荧光寿命

中图分类号: TQ174 **文献标志码:** A

Supporting Materials:

Luminescence Property and Judd-Ofelt Analysis of 0.6%Pr, *x*%La:CaF_2 Crystals

QIAN Xinyu[1,2], WANG Wudi[2], SONG Qingsong[2], DONG Yongjun[4], XUE Yanyan[2], ZHANG Chenbo[2], WANG Qingguo[2], XU Xiaodong[3], TANG Huili[2], CAO Guixin[1], XU Jun[2]

(1. Materials Genome Institute, Shanghai University, Shanghai 200444, China; 2. Key Laboratory of Advanced Micro-Structured Materials of Ministry of Education, School of Physics Science and Engineering, Institute for Advanced Study, Tongji University, Shanghai 200092, China; 3. Jiangsu Key Laboratory of Advanced Laser Materials and Devices, School of Physics and Electronic Engineering, Jiangsu Normal University, Xuzhou 221116, China; 4. Nanjing Metalaser Photonics Company Ltd., Nanjing 210038, China)

Table S1　Actual concentration of Pr^{3+} and La^{3+} ions in CaF_2 crystals

Crystal	Initial concentration/%(in atomic)		Actual concentration/%(in atomic)		Segregation coefficient	
	Pr^{3+}	La^{3+}	Pr^{3+}	La^{3+}	Pr^{3+}	La^{3+}
Pr,La:CaF_2	0.60	0.00	0.53	0.00	0.88	–
	0.60	3.00	0.52	3.06	0.86	1.02
	0.60	10.00	0.53	8.59	0.89	0.86
	0.60	18.00	0.47	15.49	0.79	0.86

Table S2　Average wavelength λ, absorption line strength $S_{exp}(J, J')$ and calculated line strength $S_{cal}(J, J')$

	0.6%Pr,3%La:CaF_2			0.6%Pr,10%La:CaF_2			0.6%Pr,18%La:CaF_2		
	λ/nm	S_{exp}/($\times10^{-20}$, cm^2)	S_{cal}/($\times10^{-20}$, cm^2)	λ/nm	S_{exp}/($\times10^{-20}$, cm^2)	S_{cal}/($\times10^{-20}$, cm^2)	λ/nm	S_{exp}/($\times10^{-20}$, cm^2)	S_{cal}/($\times10^{-20}$, cm^2)
$^3P_2$	443	1.848	0.267	443	1.617	0.209	443	2.024	0.269
$^3P_1+^1I_6$	468	0.367	0.214	468	0.376	0.238	468	0.451	0.240
$^3P_0$	483	0.145	0.130	483	0.119	0.150	482	0.240	0.150
$^1D_2$	591	0.526	0.136	590	0.580	0.111	590	0.461	0.138
$^1G_4$	1011	0.194	0.027	997	0.205	0.024	991	0.140	0.028
$^3F_4$	1443	0.699	1.011	1442	0.714	0.788	1437	0.820	1.016
$^3F_3$	1550	2.291	1.657	1554	1.727	1.420	1551	2.300	1.706
$^3F_2$	1945	1.161	0.834	1920	1.528	1.377	1936	1.380	1.021
$^3H_6$	2250	0.406	0.296	2252	0.391	0.230	2257	0.334	0.298
RMS ΔS/($\times10^{-20}$, cm^2)		0.744			0.290			0.793	

Table S3　J-O intensity parameters of Pr,La:CaF_2 crystals and other crystals

Crystal	Ω_2/($\times10^{-20}$, cm^2)	Ω_4/($\times10^{-20}$, cm^2)	Ω_6/($\times10^{-20}$, cm^2)	Ω_4/Ω_6	Ref.
0.6%Pr,3%La:CaF_2	0.59	0.76	1.94	0.39	
0.6%Pr,10%La:CaF_2	1.68	0.88	1.44	0.61	This work
0.6%Pr,18%La:CaF_2	0.87	0.87	1.93	0.45	
LaF_3	0.72	0.39	4.79	0.08	[22]
CaF_2	1.15	3.60	10.00	0.36	[23]
LYF_4	3.45	3.94	6.13	0.64	[22]
BaY_2F_8	1.09	3.49	2.22	1.57	[23]
KYF_4	3.92	1.78	7.94	0.22	[23]
$CaYAlO_4$	5.67	8.09	14.90	0.54	[26]
$YAlO_3$	2.28	3.88	5.15	0.75	[30]
$Y_3Al_5O_{12}$	0.00	12.20	8.17	1.49	[24]
$SrAl_{11}O_{19}$	0.84	2.19	6.86	0.32	[30]

Table S4 Radiative transition rates *A*, fluorescence branching ratio *β* and radiation lifetime *τ*

Crystal	Transitions from $^3P_0$	λ/nm	A_{ed}/S^{-1}	β/%	τ/μs
0.6%Pr:CaF_2	$^3H_4$	485	2068.02	28.39	137.3
	$^3H_5$	532	0.00	0.00	
	$^3H_6$	607	745.80	10.24	
	$^3F_2$	645	4081.31	56.04	
	$^3F_3$+$^3F_4$	724	387.93	5.33	
0.6%Pr,3%La:CaF_2	$^3H_4$	485	2161.59	43.48	201.1
	$^3H_5$	532	0.00	0.00	
	$^3H_6$	608	1186.02	23.85	
	$^3F_2$	644	1220.94	24.56	
	$^3F_3$+$^3F_4$	725	403.47	8.11	
0.6%Pr,10%La:CaF_2	$^3H_4$	485	8357.08	34.01	136.3
	$^3H_5$	532	0.00	0.00	
	$^3H_6$	608	3557.05	11.95	
	$^3F_2$	644	4803.69	47.68	
	$^3F_3$+$^3F_4$	725	1562.94	6.36	
0.6%Pr,18%La:CaF_2	$^3H_4$	485	559.00	41.82	168.9
	$^3H_5$	532	0.00	0.00	
	$^3H_6$	608	3642.46	19.80	
	$^3F_2$	644	769.30	30.55	
	$^3F_3$+$^3F_4$	725	104.56	7.82	

Table S5 Peak wavelength *λ*, FWHM and stimulated emission cross section σ_{em}

Concentration of La^{3+} ion	Transition	λ_{em}/nm	FWHM/nm	σ_{em}/($\times10^{-20}$, cm^2)
0.6%Pr:CaF_2	$^3P_0\rightarrow{}^3H_4$	482	5.20	0.77
	$^3P_0\rightarrow{}^3H_5$	535	26.68	0.00
	$^3P_0\rightarrow{}^3H_6$	605	15.84	1.14
	$^3P_0\rightarrow{}^3F_2$	640	5.13	0.96
	$^3P_0\rightarrow{}^3F_3$+$^3F_4$	723	4.51	0.59
0.6%Pr,3%La:CaF_2	$^3P_0\rightarrow{}^3H_4$	484	6.76	1.96
	$^3P_0\rightarrow{}^3H_5$	537	27.45	0.00
	$^3P_0\rightarrow{}^3H_6$	599	15.30	1.35
	$^3P_0\rightarrow{}^3F_2$	640	3.12	1.51
	$^3P_0\rightarrow{}^3F_3$+$^3F_4$	723	5.21	2.48
0.6%Pr,10%La:CaF_2	$^3P_0\rightarrow{}^3H_4$	484	8.36	2.52
	$^3P_0\rightarrow{}^3H_5$	535	26.76	0.00
	$^3P_0\rightarrow{}^3H_6$	599	16.98	1.36
	$^3P_0\rightarrow{}^3F_2$	640	3.80	3.18
	$^3P_0\rightarrow{}^3F_3$+$^3F_4$	723	5.49	3.03
0.6%Pr,18%La:CaF_2	$^3P_0\rightarrow{}^3H_4$	482	9.57	1.22
	$^3P_0\rightarrow{}^3H_5$	537	26.25	0.00
	$^3P_0\rightarrow{}^3H_6$	606	18.53	1.24
	$^3P_0\rightarrow{}^3F_2$	640	3.80	2.92
	$^3P_0\rightarrow{}^3F_3$+$^3F_4$	723	7.38	1.40

Table S6　Wavelength λ, FWHM, stimulated emission cross section σ_{em} and spectral quality factor $\sigma_{em}\cdot\tau_f$ for the transition of $^3P_0\rightarrow{}^3H_6$ and $^3P_0\rightarrow{}^3F_2$ of Pr,La:CaF_2 and other crystals

Crystal	Transition	FWHM/nm	σ_{em}/($\times10^{-20}$, cm^2)	τ/μs	$\sigma_{em}\cdot\tau_f$/($\times10^{-20}$, $cm^2\cdot$μs)	Ref.
0.6%Pr:CaF_2	$^3P_0\rightarrow{}^3H_6$	15.84	1.14	45.30	51.65	This work
	$^3P_0\rightarrow{}^3F_2$	5.13	0.96		43.53	
0.6%Pr,3%La:CaF_2	$^3P_0\rightarrow{}^3H_6$	15.3	1.35	45.33	61.20	
	$^3P_0\rightarrow{}^3F_2$	3.12	1.51		68.65	
0.6%Pr,10%La:CaF_2	$^3P_0\rightarrow{}^3H_6$	16.98	1.36	45.82	62.32	
	$^3P_0\rightarrow{}^3F_2$	3.80	3.18		145.79	
0.6%Pr,18%La:CaF_2	$^3P_0\rightarrow{}^3H_6$	18.53	1.24	39.75	49.29	
	$^3P_0\rightarrow{}^3F_2$	3.80	2.92		116.10	
LaF_3	$^3P_0\rightarrow{}^3H_6$	3	3.3	51.42	169.67	[22]
	$^3P_0\rightarrow{}^3F_2$	7.7	7.56		388.70	
$LuLiF_4$	$^3P_0\rightarrow{}^3H_6$	1.2	12	37.90	454.80	[33]
	$^3P_0\rightarrow{}^3F_2$	0.7	21		795.90	
$YLiF_4$	$^3P_0\rightarrow{}^3H_6$	1.4	14	35.70	499.80	[33]
	$^3P_0\rightarrow{}^3F_2$	0.7	22		785.40	
$GdLiF_4$	$^3P_0\rightarrow{}^3H_6$	1.3	13	43.61	566.91	[33]
	$^3P_0\rightarrow{}^3F_2$	–	23		1003.00	
BaY_2F_8	$^3P_0\rightarrow{}^3H_6$	1.2	24.7	43.00	1062.10	[32]
	$^3P_0\rightarrow{}^3F_2$	0.6	12.1		520.30	